

AN ALMA VIEW OF MOLECULAR FILAMENTS IN THE LARGE MAGELLANIC CLOUD II: AN EARLY STAGE OF HIGH-MASS STAR FORMATION EMBEDDED AT COLLIDING CLOUDS IN N159W-SOUTH

KAZUKI TOKUDA,^{1,2} YASUO FUKUI,³ RYOHEI HARADA,¹ KAZUYA SAIGO,² KENGO TACHIHARA,³ KISETSU TSUGE,³ TSUYOSHI INOUE,³ KAZUFUMI TORII,⁴ ATSUSHI NISHIMURA,³ SAROLTA ZAHORECZ,^{1,2} OMNARAYANI NAYAK,⁵ MARGARET MEIXNER,^{5,6} TETSUHIRO MINAMIDANI,⁴ AKIKO KAWAMURA,² NORIKAZU MIZUNO,^{2,7} REMY INDEBETOUW,^{8,9} MARTA SEWILO,^{10,11} SUZANNE MADDEN,¹² MAUD GALAMETZ,¹² VIANNEY LEBOUTELLER,¹² C.-H. ROSIE CHEN,¹³ AND TOSHIKAZU ONISHI¹

¹*Department of Physical Science, Graduate School of Science, Osaka Prefecture University, 1-1 Gakuen-cho, Naka-ku, Sakai, Osaka 599-8531, Japan*

²*Chile Observatory, National Astronomical Observatory of Japan, National Institutes of Natural Science, 2-21-1 Osawa, Mitaka, Tokyo 181-8588, Japan*

³*Department of Physics, Nagoya University, Chikusa-ku, Nagoya 464-8602, Japan*

⁴*Nobeyama Radio Observatory, 462-2 Nobeyama Minamimaki-mura, Minamisaku-gun, Nagano 384-1305, Japan*

⁵*Department of Physics & Astronomy, Johns Hopkins University, 3400 N. Charles Street, Baltimore, MD 21218, USA*

⁶*Space Telescope Science Institute, 3700 San Martin Drive, Baltimore, MD 21218, USA*

⁷*Department of Astronomy, School of Science, The University of Tokyo, 7-3-1 Hongo, Bunkyo-ku, Tokyo 113-0033, Japan*

⁸*Department of Astronomy, University of Virginia, P.O. Box 400325, Charlottesville, VA 22904, USA*

⁹*National Radio Astronomy Observatory, 520 Edgemont Road, Charlottesville, VA 22903, USA*

¹⁰*CRESST II and Exoplanets and Stellar Astrophysics Laboratory, NASA, Goddard Space Flight Center, Greenbelt, MD 20771, USA*

¹¹*Department of Astronomy, University of Maryland, College Park, MD 20742, USA*

¹²*AIM, CEA, CNRS, Université Paris-Saclay, Université Paris Diderot, Sorbonne Paris Cité, F-91191 Gif-sur-Yvette, France*

¹³*Max Planck Institute for Radio Astronomy, Auf dem Huegel 69, D-53121 Bonn, Germany*

(Received November 13, 2018)

Submitted to ApJ

ABSTRACT

We have conducted ALMA CO isotopes and 1.3 mm continuum observations toward filamentary molecular clouds of the N159W-South region in the Large Magellanic Cloud with an angular resolution of $\sim 0''.25$ (~ 0.07 pc). Although the previous lower resolution ($\sim 1''$) ALMA observations revealed that there is a high-mass protostellar object at an intersection of two linear-shaped filaments in ^{13}CO with the length scale of ~ 10 pc (Fukui et al. 2015), the spatially resolved observations, in particular, toward the highest column density part traced by the 1.3 mm continuum emission, the N159W-South clump, show complicated hub-filamentary structures. We also discovered that there are multiple protostellar sources with bipolar outflows along the massive filament. The redshifted/blueshifted components of the ^{13}CO emission around the massive filaments/protostars show complementary distributions to each other, which is considered to be a possible piece of evidence for a cloud-cloud collision. We propose a new scenario that the supersonically colliding gas flow triggered the formation of both the massive filament and protostars. This is a modification of the earlier scenario of cloud-cloud collision which postulated the two filamentary clouds prior to the high-mass star formation by Fukui et al. (2015). A recent theoretical study of the shock compression in colliding molecular flows by Inoue et al. (2018) demonstrates that the formation of filaments with hub-structure is a usual outcome of the collision, lending support for the present scenario. In the theory the filaments are formed as dense parts in a shock compressed sheet-like layer, which resembles “an umbrella with pokes”.

Keywords: stars: formation — stars: high-mass — stars: protostars — ISM: clouds— ISM: kinematics
and dynamics — ISM: individual (N159W)

1. INTRODUCTION

Despite high-mass stars are considered to have great effects on the galaxy evolution, their formation process is not fully understood. There are a number of works which investigated the high-mass star formation mechanism (for reviews, e.g., Zinnecker & York 2007; Tan et al. 2014). Although the precursors of massive stars are supposed to be very dense and massive ($\sim 100 M_{\odot}$) cores (e.g., Krumholz et al. 2009; Peretto et al. 2013), it may be a problem how such peculiar cores are formed as an initial condition of massive star formation. Habe & Ohta (1992) suggested that molecular cloud collision form a dense shock compressed layer, which is massive enough to form massive star based on their numerical simulations in a short timescale less than 1 Myr (see also, Takahira et al. 2014; Matsumoto et al. 2015; Shima et al. 2017). Inoue et al. (2018) demonstrated that shock compressions induced by the cloud-cloud collision promote massive filament formation, which is perpendicular to the background magnetic field (see also Inoue & Fukui 2013). O-type stars are formed by the global collapse of the massive filament with high-accretion rate, $>10^{-4} M_{\odot} \text{ yr}^{-1}$. Since the high-mass protostars are supposed to be formed in giant molecular clouds (GMCs), detailed observational studies toward the GMCs are thus needed to examine the initial conditions of high-mass star formation. Large-scale surveys with high-angular resolution ($<0.1\text{--}1$ pc) in the Galaxy have been providing us with fruitful knowledge on the physical properties of molecular clouds and (high-)mass star formation. Recent high-angular resolution observations with ground-based single-dish telescopes and the *Herschel* satellite revealed that filamentary structures are ubiquitous in both dark clouds and GMCs (e.g., Mizuno et al. 1995; Nagahama et al. 1998; Arzoumanian et al. 2011, 2018; André et al. 2014, 2016). High-mass young stellar objects (YSOs) tend to be located at the intersection of multiple filamentary clouds, called “hub-filament” (e.g., Myers 2009; Peretto et al. 2013). The central part of hub-filaments is as massive as $\gtrsim 1000 M_{\odot} \text{ pc}^{-1}$, which is sometimes referred to as “ridge” (e.g., Motte et al. 2007; Hill et al. 2012; Nguyen-Lu’o’ng et al. 2013). Because the line mass of the ridges is significantly higher than the critical line mass of an isothermal filament (c.f., Inutsuka & Miyama 1997), by up to two orders of magnitude, they are supposed to be very unstable against the global collapse and fragmentation. Although some formation/stabilization mechanism of the hub-filaments and the ridges, such as large-scale compression and internal MHD (magneto-hydrodynamic) waves, have been proposed (André et al. 2016), the true nature is not fully understood so far possibly due to the lack of the suitable targets in the solar neighborhood.

ALMA has great capabilities to resolve internal structures of molecular clouds even in external galaxies. In particular, the Large Magellanic Clouds (LMC) is an ideal laboratory to investigate high-mass star formation thanks to the nearly face-on view (Balbinot et al. 2015) and the close distance, ~ 50 kpc (Schaefer 2008; de Grijs et al. 2014). It is also a great advantage to directly compare the distributions of molecular gas observed by ALMA and positions of massive YSOs identified by *Spitzer* and *Herschel* (e.g., Gruendl & Chu 2009; Chen et al. 2010; Seale et al. 2014) without any concerns about serious contamination in the line of sight. Earlier studies using the H I gas observations found that there are supergiant shells (Kim et al. 1999, 2003) and kpc scale gas flows caused by the last tidal interaction between the LMC and the Small Magellanic Clouds (SMC) (Fukui et al. 2017). Therefore, we may be able to examine the relation between such large-scale gas kinematics and the local star formation activities. Our present target in this paper is the N159W-South clump, which was discovered by our previous ALMA Cycle 1 observations (Fukui et al. 2015), hereafter Paper I) with an angular resolution of $\sim 1''$ (~ 0.24 pc) toward a GMC in the N159W region (e.g., Johansson et al. 1998; Minamidani et al. 2008, 2011). Paper I revealed that the GMC is composed by many filamentary molecular clouds and discovered the first example of protostellar outflows in the external galaxies. Paper I also found that the protostellar source with the stellar mass of $\sim 37 M_{\odot}$ in the N159W-South clump is located toward an intersection of two filaments and suggested that the filament-filament collision triggered the protostar formation. Although the ALMA observations significantly improved our understanding of molecular clouds structures and star formation in this object, much higher angular resolution studies are needed to further resolve the filamentary structures with a width of ~ 0.1 pc (c.f., Arzoumanian et al. 2011, 2018) and investigate the star formation activities therein. In this paper, we present high-angular resolution observations with $\sim 0''.25$ (~ 0.07 pc) resolution toward the N159W-South clump in the ALMA Cycle 4 (P.I.: Y. Fukui #2016.1.01173.S). We also observed the N159W-North and the N159E-Papillon region in the same project. The observational results of the N159E-Papillon region, which is considered to be in a later evolutionary stage than the N159W-South clump (Saigo et al. 2017), are presented in a separate paper (Fukui et al. 2018b submitted, hereafter FTS18).

2. OBSERVATIONS

We carried out ALMA Cycle 4 Band 6 (211–275 GHz) observations toward the N159W with the main array 12 m antennas. The observations of N159W-South centered at $(\alpha_{J2000.0}, \delta_{J2000.0}) = (5^{\text{h}}39^{\text{m}}41^{\text{s}}.0, -69^{\circ}46'06''.0)$ were carried out between 2016 November and 2017 July. There were three spectral windows targeting ^{12}CO ($J = 2-1$), ^{13}CO ($J = 2-1$) and C^{18}O ($J = 2-1$) with a bandwidth of 58.6 MHz. The frequency resolutions were 30.6 kHz for ^{12}CO ($J = 2-1$) and 61.0 kHz for the others. We used two spectral windows for the continuum observations with the aggregated bandwidth of 3.75 GHz. The observed frequencies include some line emission, such as the radio recombination line of $\text{H}30\alpha$ and SiO ($J = 5-4$). The projected baseline length ranges from 14 to 1940 m. We also observed two other objects in N159, the N159W-North, and the N159-Papillon region. The detailed result of the N159E-Papillon region is described in a separate paper (FTS18).

The data were processed with the CASA (Common Astronomy Software Application) package (McMullin et al. 2007) version 5.0.0. We used the briggs weighting with the robust parameter of 0.5. The synthesized beams of the continuum and the ^{13}CO ($J = 2-1$) observations are $0''.26 \times 0''.23$ and $0''.29 \times 0''.25$, respectively. The (1σ) RMS noise levels of the line and the 1.3 mm continuum are $\sim 4.5 \text{ mJy beam}^{-1}$ ($\sim 1.5 \text{ K}$) at a velocity resolution of 0.2 km s^{-1} and $\sim 0.027 \text{ mJy beam}^{-1}$. We concluded that the previous ALMA Cycle 1 observations (Paper I, see also Nayak et al. 2018) did not show significant missing flux of this source based on the comparison between the ALMA and the single-dish observations. The total fluxes of the ^{12}CO , ^{13}CO and the 1.3 mm continuum data of the Cycle 4 were $\sim 20\%$ lower than those of the Cycle 1. Because the current observations fully cover the baseline range of the previous one, 16–395 m, the discrepancies are supposed to be mainly caused by the calibration error instead of the missing flux. We thus use the Cycle 4 data alone in the following analysis in this paper.

3. RESULTS

3.1. 1.1 Multiple protostellar sources with outflows

Figures 1 (a-c) show 1.3 mm dust continuum and ^{13}CO ($J = 2-1$) distributions in the N159W-South clump. We find three major continuum peaks, MMS-1, 2 and 3 along the filamentary structure. The local peaks were not spatially resolved with our previous lower resolution study with an angular resolution of $\sim 1''$ (Paper I). The positions of MMS-1 and MMS-2 correspond to near-infrared sources, 121 and 123, respectively, discovered by the VLT (Very Large Telescope) observations (Testor et al. (2006), see also the Gemini observations by Bernard et al. (2016)). MMS-3 has no counterpart in the infrared observations, indicating that this source is the youngest one among the dust condensations. We assumed the absorption coefficient per unit dust mass at 1.3 mm, the dust-to-gas mass ratio and the dust temperature to be $0.77 \text{ cm}^2 \text{ g}^{-1}$, 3.5×10^{-3} , and 20 K, respectively, to derive the gas mass from the dust emission (c.f., Herrera et al. 2013; Paper I). The total mass of the filamentary structure traced by the dust continuum is $\sim 4 \times 10^3 M_{\odot}$ (see also Paper I) and those of the local peaks are a few $\times 10^2 M_{\odot}$, respectively. The spatial separations among the dust peaks are roughly $\sim 0.2 \text{ pc}$. The total length and the averaged width (FWHM) of the dust filament are $\sim 1.7 \text{ pc}$ and $\sim 0.14 \text{ pc}$, respectively. The resultant line mass of the filament is $\sim 2 \times 10^3 M_{\odot} \text{ pc}^{-1}$. These properties are consistent with those of “ridges” in Galactic high-mass star-forming clouds (e.g., NGC6334, André et al. 2016).

The ^{12}CO ($J = 2-1$) observations have detected compact high-velocity wings tracing outflow motion from the protostellar outflows (Figures 1 (b-g)). For the panel (c) sources, the previous ^{12}CO observations identified these multiple flows as a single bipolar flow due to the lack of the angular resolution (Figure 2 in Paper I). The blue/red wings from MMS-1 and MMS-2 are possibly merged as shown in Figure 1 (c). Especially for the blue component, it is hard to separate the individual components, we plotted the same spectra in the Figures 1 (f,g) and listed as the blue wing of MMS-1. We also discovered a new bipolar outflow embedded in the ^{13}CO filament without the dust continuum and infrared emission (Figures 1(a,b,d)). This strongly indicates that there is a protostellar source (hereafter, YSO-SN) located at the central position of the outflow. The physical parameters of these outflows are listed in Table 1. We calculated the outflow force (F_{CO}) by using the procedure in Beuther et al. (2002). The relations between the F_{CO} and the core mass derived from the dust emission for MMS-1, 2, and 3 roughly follow those seen at massive protostellar sources in the Galaxy (Beuther et al. 2002). Although we could not detect dust emission from YSO-SN, this is also considered to be a massive source because the outflow parameters are very similar to those of the other massive sources. We thus conclude that the multiple protostellar sources with separations of $\sim 0.2-2 \text{ pc}$ are forming along the filamentary cloud without significant time delay more than $\sim 10^4 \text{ yr}$ based on the dynamical time of the outflows (Table 1). We also found similar star formation activities in the N159E-Papillon region (FTS18). Note that the directions of the outflows in the N159W-South clump are roughly perpendicular to the orientation of the filament, indicating that

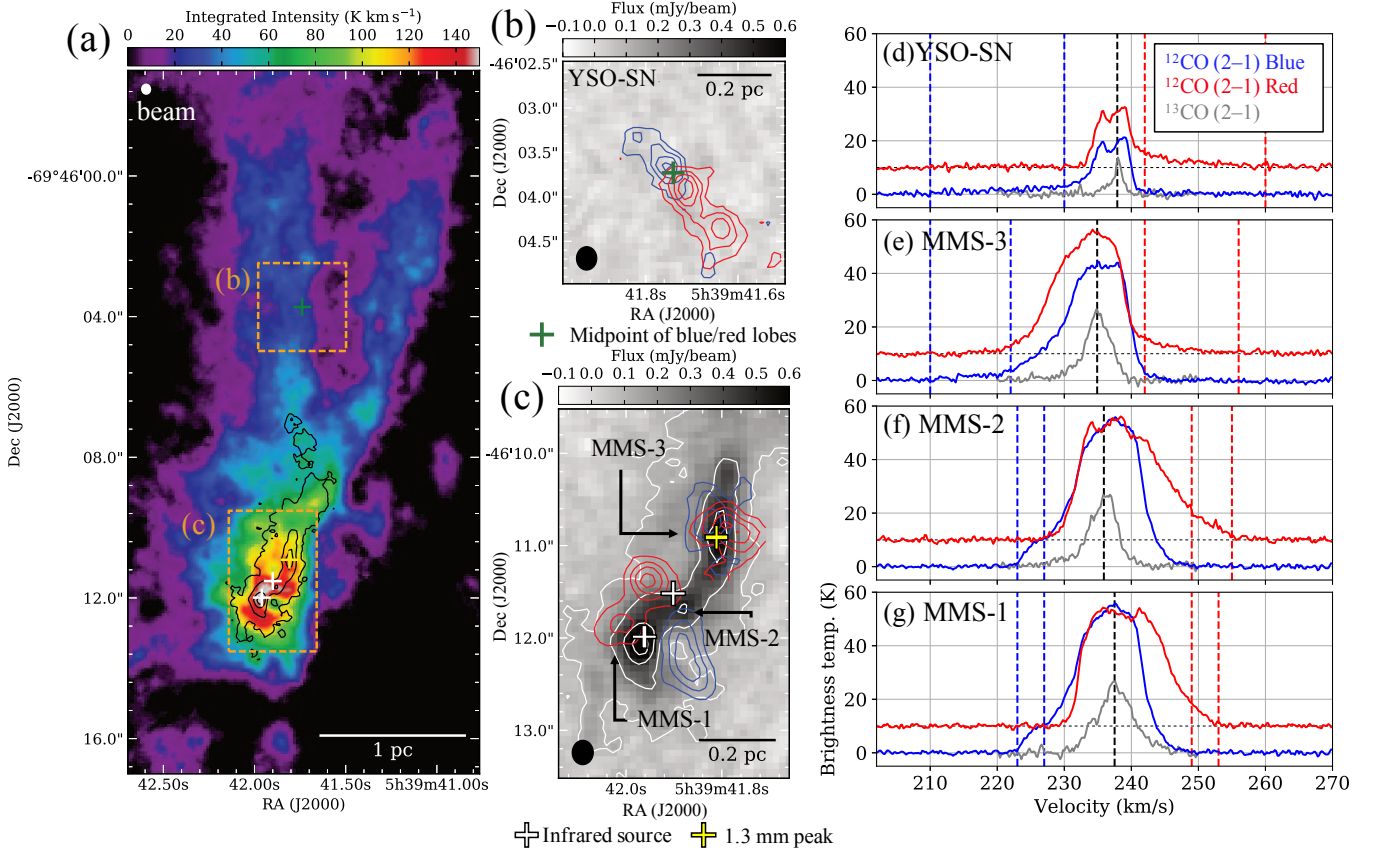


Figure 1. Multiple outflows along the filamentary structure toward the N159W-South clump. (a) Color-scale image and black contours show the total velocity-integrated intensity map in ^{13}CO ($J = 2-1$) and the 1.3 mm continuum emission. The minimum contour level and the subsequent steps are 0.1 and 0.2 mJy beam^{-1} , respectively. The angular resolution, $0''.26 \times 0''.23$, is given by the ellipse in upper left corner. The white crosses represent the positions of the infrared sources identified with the VLT observations (Testor et al. 2006). The yellow and green crosses denote the dust continuum peak of MMS-3 and the median position between the redshifted and blueshifted outflow lobes shown in panel (b), respectively. (b,c) Redshifted and blueshifted outflow lobes in ^{12}CO ($J = 2-1$) are shown in blue and red contours, respectively. The contour levels are 10, 20, 30, and 40 K km s^{-1} . The integrated-velocity ranges are shown in dashed lines in panels (d-g). Grayscale images and white contours show the 1.3 mm continuum emission same as panel (a). (d-g) Red and blue lines show averaged spectra of the outflow wings for MMS-1,2,3 and YSO-SN over the regions inside the lowest red and blue contours, respectively, in (b) and (c). Note that the same spectra are plotted as the blue wings in panel (f,g) (see the text). The red lines are offset by +10 K for the visualization. Gray lines show the ^{13}CO ($J = 2-1$) spectra at the position of the protostellar sources shown in panel (b,c). Black lines indicate the central velocities obtained by fitting the ^{13}CO ($J = 2-1$) spectra with a single Gaussian profile at the dust peaks for MMS-1,2,3 and the cross position in the panel (b) for YSO-SN.

the magnetic field directions are also perpendicular to that. We discuss the formation scenario of the YSOs and the filament in Sect. 4.

3.2. Velocity and spatial structures of the filamentary clouds

We present the velocity/spatial distributions of the ^{13}CO filamentary clouds toward the N159W-S clump. Figure 2 represents the channel maps of the ^{13}CO ($J = 2-1$) observations with the contours of the 1.3 mm continuum as shown in Figure 1. The velocity/spatial distributions of the ^{13}CO clouds have the rich structures rather than two simple filamentary clouds as previously reported based on the lower resolution observations (Figure 3 in Paper I). Furthermore, we also identify hub features elongated toward the dust filament and the YSOs in the velocity channel of $\sim 237 \text{ km s}^{-1}$ (the lower left panel in Figure 2). Similar morphologies are seen in the Galactic high-mass star-forming clumps (e.g., Motte et al. 2007; Peretto et al. 2013; Williams et al. 2018). We calculated the column densities by using the ^{13}CO ($J = 2-1$) data assuming the Local thermo-dynamical equilibrium (see also the detailed procedure in

Table 1. Outflow properties

Source name	Outflow lobe	Mass ^a (M_{\odot})	Distance ^b (pc)	Velocity ^c (km s^{-1})	t_d ^d (yr)
MMS-1	Blue lobe ^e	7.2	0.13	14.5	$5.1\text{--}25 \times 10^3$
	Red lobe	2.8	0.07	15.5	$2.6\text{--}13 \times 10^3$
MMS-2	Red lobe	3.4	0.12	19.1	$3.6\text{--}17 \times 10^3$
MMS-3	Blue lobe	4.4	0.06	24.9	$1.4\text{--}6.5 \times 10^3$
	Red lobe	4.5	0.05	21.1	$1.3\text{--}6.1 \times 10^3$
YSO-SN	Blue lobe	1.5	0.17	22.1	$4.3\text{--}20 \times 10^3$
	Red lobe	3.2	0.17	27.9	$3.4\text{--}16 \times 10^3$

^a The outflow mass is estimated from the ^{12}CO ($J = 2\text{--}1$) intensity by assuming a conversion factor from ^{12}CO ($J = 1\text{--}0$) intensity to the column density of $X_{\text{CO}} = 7 \times 10^{20} \text{ cm}^{-2} (\text{K km s}^{-1})^{-1}$ (Fukui et al. 2008) and the ^{12}CO ($J = 2\text{--}1$)/ ^{12}CO ($J = 1\text{--}0$) ratio = 1.0.

^b Projected distances to the peak intensity of the outflow lobes from the continuum peak of each mm-source for MMS-1,2, and 3. For YSO-SN, the distances from the cross position in Figure 1 (b) to the second peak of each outflow lobe.

^c Maximum radial velocity of the outflow lobe with respect to the systemic velocity (see also black lines in Figures 1 (d-g)).

^d Dynamical time is estimates as the distances divided by the velocity by assuming the inclination angles of 30–70 degree.

^e This blue lobe is considered to be merged with that from MMS-2 (see the text and Figure 1).

FTS18). The column density, line mass, and width of the typical filaments are $\sim 10^{22}\text{--}10^{23} \text{ cm}^{-2}$, a few hundred M_{\odot} , and $\sim 0.1 \text{ pc}$, respectively, except for the highest column density part with the 1.3 mm continuum detection. These filaments are significantly more massive than those in the solar neighborhood (c.f., Arzoumanian et al. 2011) and close to those in high-mass star-forming region (e.g., Vela C, Hill et al. 2012).

The velocity analysis of the ^{13}CO data found that the blueshifted ($230.0\text{--}233.2 \text{ km s}^{-1}$) and redshifted ($239.0\text{--}242.0 \text{ km s}^{-1}$) components show the complementary distributions to each other (Figure 3 (a)). The first-moment intensity-weighted velocity map using the full-velocity range of the ^{13}CO data also shows similar trend. Complementary gas distributions are often seen in regions with cloud-cloud collision events (e.g, Matsumoto et al. 2015; Torii et al. 2007; Tokuda et al. 2018; Fukui et al. 2018c).

The PV diagram shows (Figure 3(b)) two high-velocity components with the V-shaped features shown in the green dotted lines toward the three YSOs, the redshifted one for MMS-1 and the blueshifted ones for MMS-2,3. Although these velocity features were seen as a broad linewidth component with the velocity span of $\sim 10 \text{ km s}^{-1}$ at a resolution of $\sim 0.3 \text{ pc}$, the current high-resolution data clearly resolved the V-shape features associated with the individual YSOs. The high-velocity components may not be explained by the outflow activities alone because there are no counterparts toward the each opposite velocity direction. Numerical simulations (Takahira et al. 2014) and the synthetic observations (Fukui et al. 2018a) of colliding clouds also reproduced similar V-shaped structures on the P-V diagram. The present gas characteristics are consistent with the previous cases regarding the cloud-cloud collision as the trigger of massive star formation.

4. DISCUSSIONS

In this section, we discuss the formation scenario of the high-mass protostars and the filamentary molecular clouds in the N159W-South region. The line masses of the filaments in this region are large as $\sim \text{a few} \times 10^2\text{--}10^3 M_{\odot} \text{ pc}^{-1}$. Such kinds of massive filaments should be in a “supercritical” state (c.f., Inutsuka & Miyama 1997), and are considered to fragment and radially collapse within the free-fall time. We speculate that the massive filaments what we see in the present observations are formed quite recently and may be transient objects (see also discussions in André et al. 2016). The short dynamical time of the outflows (Sect. 3.1) and the reddening of the protostellar sources for MMS-1, and MMS-2 (Testor et al. 2006; Bernard et al. 2016) strongly indicate that the YSOs are in an extremely young phase within $\sim 10^4$ yrs after the protostar formation. Therefore, there is a possibility that the filaments and the protostars were formed at almost the same time. We previously discussed that a collision between two massive

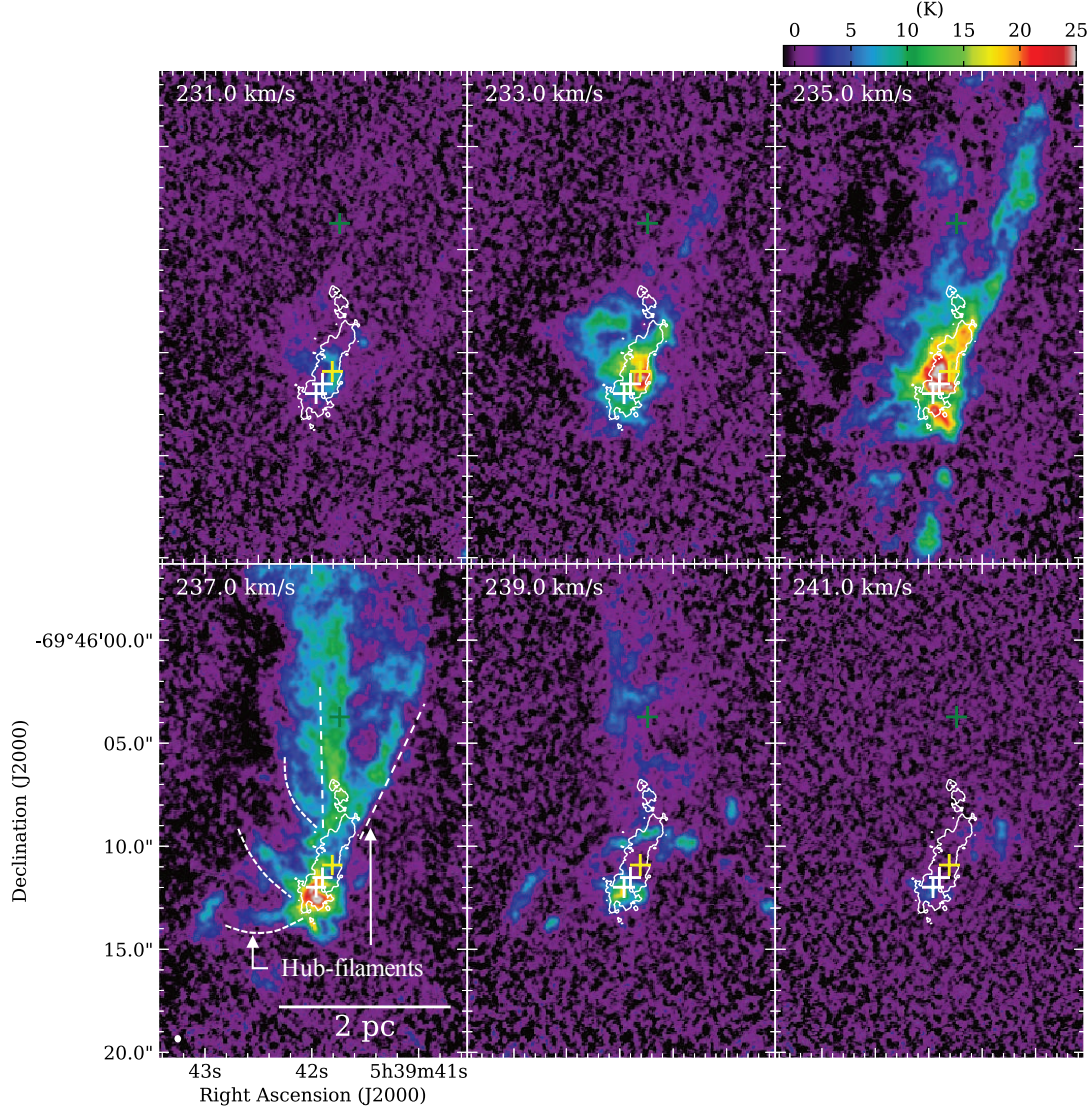


Figure 2. Velocity-channel maps toward the N159W-South clump in ^{13}CO ($J = 2-1$). The lowest velocities are given in the upper left corners in each panel. White contours show the 1.3 mm continuum emission, as shown in Figure 1. The contour level is $0.1 \text{ mJy beam}^{-1}$. The angular resolution is given as a white ellipse in the lower left of the left panel, $0''.28 \times 0''.25$. White, yellow and green crosses are same as Figure 1.

filaments with the line mass of a few $\times 100 M_{\odot}$ triggered the massive star formation in this region (Paper I). However, such simple model of two colliding filaments may be hard to reconcile with the complex hub-filaments revealed by the present observations. We alternatively propose that the filaments in this region have initially the hub morphology at the formation phase. Although similar massive filaments associated with several sub-filaments are reported in the Galactic massive star-forming regions (see Sect. 1, and 3.2), the formation mechanism is not fully understood so far. Some earlier studies suggest that they may be a consequence of large-scale collapse/flow of a significant portion of GMCs (Hartmann & Burkert 2007; Schneider et al. 2010). In the N159 region, another star-forming filament, the N159E-Papillon region, with similar filament morphology and star-formation activity is located at $\sim 50 \text{ pc}$ away from the N159W-South region (Saigo et al. 2017; FTS18). We thus discuss a possibility that a large-scale ($> 100 \text{ pc}$) colliding event rather than the local $\sim 10 \text{ pc}$ motion on the filament triggered the formation of filaments and high-mass protostars in this region. Inoue et al. (2018) performed numerical simulations of colliding clouds with magnetic field and turbulence and demonstrated that the turbulent inhomogeneous cloud is compressed by the shock wave and hub-filaments are developed within a few $\times 0.1 \text{ Myr}$ after the collision. The first protostar (sink particle) is created in a few

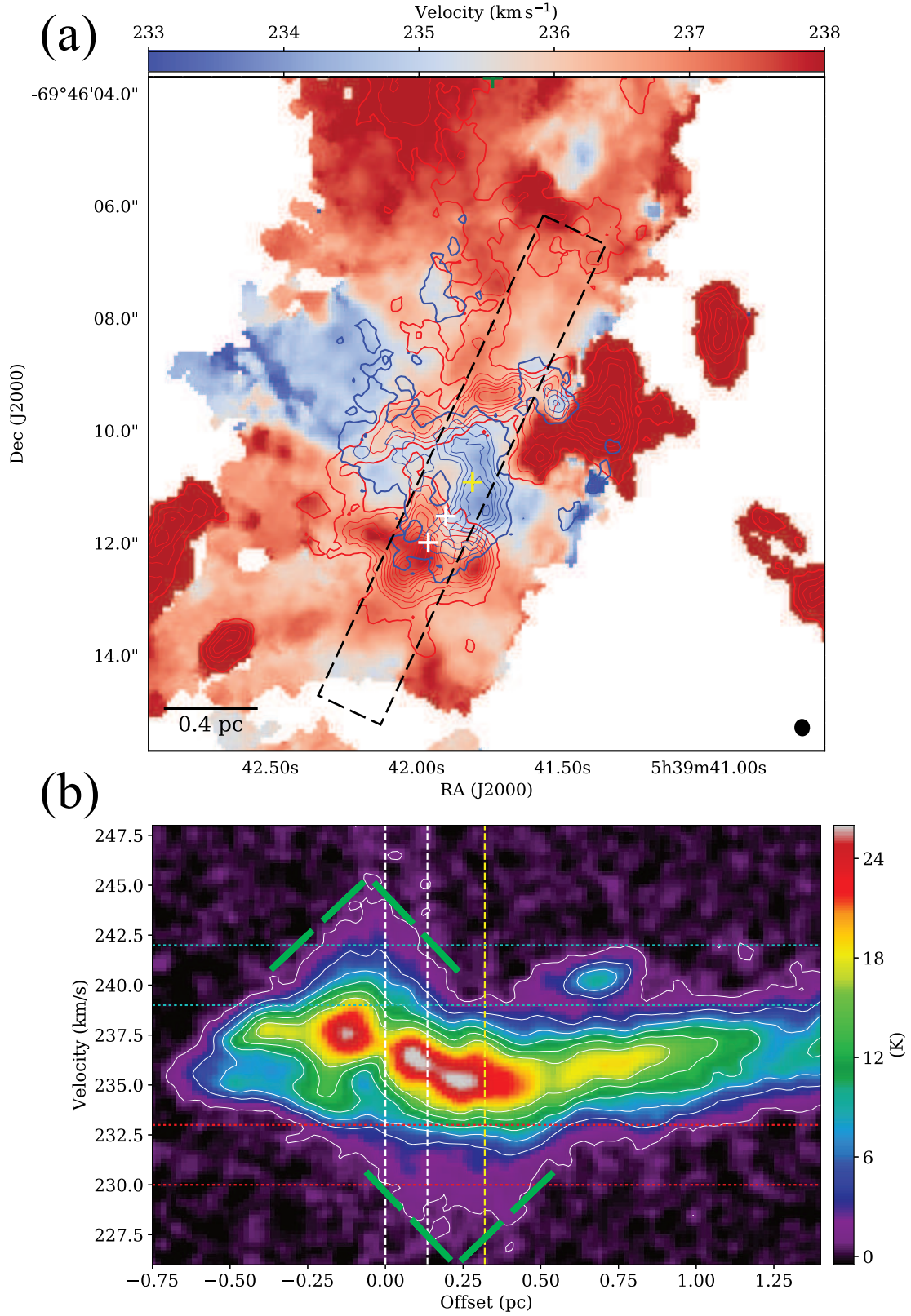


Figure 3. Velocity structures in ^{13}CO ($J = 2-1$) toward the N159W-South clump. (a) The first-moment intensity-weighted velocity map of ^{13}CO ($J = 2-1$) is shown in color scale. Blue and red contours show the velocity-integrated intensity of ^{13}CO ($J = 2-1$) with a range of $230.0\text{--}233.0 \text{ km s}^{-1}$ and $239.0\text{--}242.0 \text{ km s}^{-1}$. The lowest contour level and the subsequent contour step are 3 K km s^{-1} and 4 K km s^{-1} , respectively. White and yellow crosses are same as Figure 1. The angular resolution is given by the ellipse in the lower right corner. (b) A ^{13}CO ($J = 2-1$) position-velocity diagram along the regions shown by the dashed rectangle in panel (a). The X-axis represents angular distances in pc from the position of the YSO at MMS-1. The vertical dashed lines in panel (b) represents the position of the YSOs. The cyan and red horizontal lines show the velocity ranges for the blueshifted and redshifted components, respectively, in panel (a).

$\times 10^4$ yrs after the development of the filaments. A possible picture of star formation expected from the theoretical study and the current observations is schematically shown in Figure 4. Although there are no large differences of the dynamical time of the outflows toward each protostellar source more than $\sim 10^4$ yrs, the evolutionary stage of the northern two YSOs are supposed to be younger than the other YSOs based on the detection of the infrared emission (Figures 1 and 4). This distribution is qualitatively explained if the initial small cloud collided with the extended cloud (Inoue et al. 2018) and the star-formation took place as the propagation of the interaction layer. The evolutionary sequence is also consistent with that in the N159E-Papillon region where the compact H II region is growing at the southern edge of the filamentary clouds (FTS18).

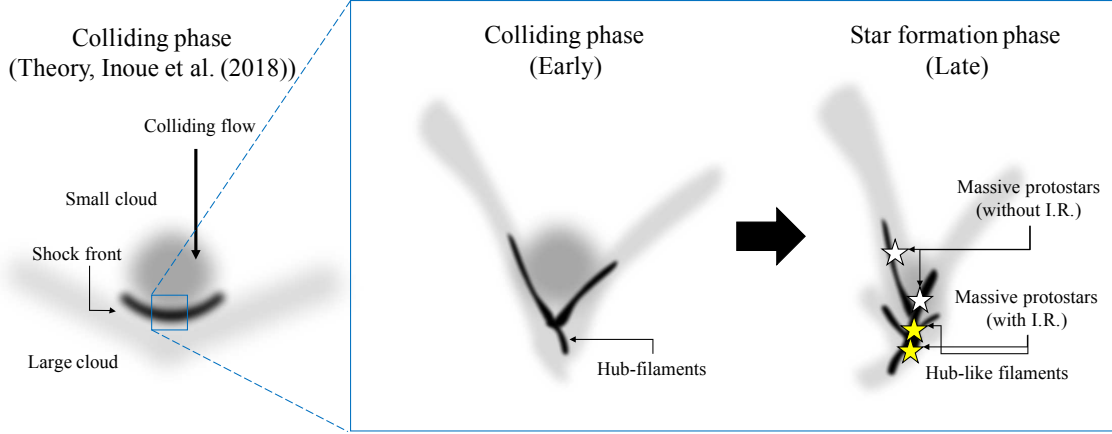


Figure 4. Schematic views of the star formation triggered by a cloud-cloud collision in the N159W-South. A similar figure is presented by FTS18.

According to numerical simulations Inoue et al. (2018), large relative velocity difference between the colliding clouds on the order of 10 km s^{-1} are needed to promote high-mass star formation activities (see also Inoue & Fukui 2013). The systematic search of large H I structures in the LMC (Kim et al. 1999) found that the N159 region is located along the western edge of an H I supergiant shell, SGS19 with a radius of $\sim 390 \text{ pc}$ and an expansion velocity of $\sim 25 \text{ km s}^{-1}$ (Dawson et al. 2013). More recently, Fukui et al. (2017) pointed out that the molecular ridge, the most massive molecular complex in the LMC, containing the N159 region was formed by large-scale H I gas flows with a relative velocity of $\sim 50 \text{ km s}^{-1}$ induced by the last galactic tidal interaction between the LMC and the SMC. Such high-velocity H I flow may be a promising candidate as the origin of strong shock compression to produce the massive filaments and massive protostars. The discrepancy between the current low velocity (a few km s^{-1}) seen in the ^{13}CO observations and the high-velocity (a few $\times 10 \text{ km s}^{-1}$) large-scale H I gas flow can be qualitatively explained by deceleration of shock velocities in the high-density CO detected region (Fukui et al. 2018c; see also Inoue & Inutsuka 2012; Inoue & Fukui 2013). The current velocity dispersion toward the high-mass star-forming filament shown in Figure 3 is not largely contradictory to that predicted on the size scale following the Larson’s law (Larson et al. 1981). Despite the fact, we still find peculiar velocity features, which is considered to be formed by a colliding motion (Sect. 3.2). These structures may represent the decelerated remnant that was originally formed by the H I flow with much larger velocity. We note that there is an issue regarding the formation time-scale of H_2 molecules if the large-scale H I compression quickly creates the molecular filaments traced by the CO observations. The formation timescale of H_2 molecules from H atoms on dust grains is considered to be as long as $\sim 10^7$ yrs with an atomic gas density of 10^2 cm^{-2} (Hollenbach & Salpeter 1971; Jura 1974), which is much longer than that of the filament formation as discussed above. According to synthetic observations (Fukui et al. 2018c) based on numerical simulations of molecular cloud formation by H I flows (Inoue & Inutsuka 2012) showed that the molecular fraction becomes 10% within a few $\times 0.1 \text{ Myr}$ after the shock compression. It is possible, in principle, to make $\sim 10^4 M_\odot$ molecular filaments after the H I gas flow if there is a sufficient mass reservoir around the filamentary cloud. Spatially resolved H I gas observations will be a future subject to better understand the high-velocity H I flows as the origin of the massive filaments. Another interesting feature is that the orientations of the observed outflows are roughly perpendicular to that of the

filament (Sect. 3.1). This may represent that the directions of magnetic fields are also perpendicular to the filament if the outflows were launched along the magnetic field direction. Simulations in Inoue et al. (2018) suggest that the magnetic field strength is significantly enhanced at the post-shock layer and massive filaments become perpendicular to the magnetic field. In an observational aspect, for example, Palmeirim et al. (2013) revealed that high-density filaments are perpendicular to the magnetic fields, while low-density striations are parallel in low-mass star-forming filaments in Taurus. Future polarization observations toward the N159W-South clump with ALMA may provide us with further evidence of the cloud-cloud collision as the trigger of the massive filament/protostar formation.

5. SUMMARY

We have carried out ALMA observations with an angular resolution of $\sim 0''.25$ (~ 0.06 pc) toward the N159W-South region in the LMC. The 1.3 mm dust continuum traces a clear filamentary feature with the line mass of $\sim 2 \times 10^3 M_\odot$ and it has three local peaks with the strong indication of outflow activities. We have identified a new bipolar outflow source embedded at a ^{13}CO filament but it is located at ~ 2 pc away from the massive dust filament. We have revealed an early stage of multiple high-mass star formation as two additional outflow sources along the filamentary cloud. The molecular line observations in ^{13}CO ($J = 2-1$) revealed the complex hub structures toward the dust filament rather than simple linear filaments as reported in our previous lower resolution observations. We propose that the massive protostars and filaments are formed by the large-scale flow, which is consistent with the recent theoretical simulations.

We thank Doris Arzoumanian and Shu-ichiro Inutsuka for discussions about the filamentary molecular clouds. This paper makes use of the following ALMA data: ADS/ JAO.ALMA#2016.1.01173.S. ALMA is a partnership of the ESO, NSF, NINS, NRC, NSC, and ASIAA. The Joint ALMA Observatory is operated by the ESO, AUI/NRAO, and NAOJ. This work was supported by NAOJ ALMA Scientific Research Grant Numbers 2016-03B and JSPS KAKENHI (Grant No. 22244014, 23403001, 26247026, and 18K13582). The work of M.S. was supported by NASA under award number 80GSFC17M0002.

REFERENCES

- André, P., Di Francesco, J., Ward-Thompson, D., et al. 2014, in *Protostars and Planets VI*, ed. H. Beuther et al. (Tucson, AZ: Univ. Arizona Press), 27
- André, P., Revéret, V., Könyves, V., et al. 2016, *A&A*, 592, A54
- Arzoumanian, D., André, P., Didelonet, P. et al. 2011, *A&A*, 529, L6
- Arzoumanian, D., André, P., Könyves, V., et al. 2018, arXiv:1810.00721
- Balbinot, E., Santiago, B. X., Girardi, L., et al. 2015, *MNRAS*, 449, 1129
- Bernard, A., Neichel, B., Samal, M. R., et al. 2016, *A&A*, 592, A77
- Beuther, H., Schilke, P., Sridharan, T. K. *A&A*, 383, 892
- Chen, C.-H. R., Indebetouw, R., Chu, Y.-H., et al. 2010, *ApJ*, 721, 1206
- Dawson, J. R., McClure-Griffiths, N. M., Wong, T., et al. 2013, *ApJ*, 763, 56
- de Grijs, R., Wicker, J. E., & Bono, G. 2014, *AJ*, 147, 122
- Fujii, K., Minamidani, T., Mizuno, N., et al. 2014, *ApJ*, 796, 123
- Fukui, Y., Harada, R., Tokuda, K., et al. 2015, *ApJL*, 807, L4
- Fukui, Y., Hayakawa, T., Inoue, T., et al. 2018a, *ApJ*, 860, 33
- Fukui, Y., Kawamura, A., Minamidani, T., et al. 2008, *ApJS*, 178, 56
- Fukui, Y., Tokuda, K., Saigo, K., et al. 2018b, arXiv:1811.00812
- Fukui, Y., Torii, K., Hattori, Y., et al. 2018c *ApJ*, 859, 166
- Fukui, Y., Torii, K., Ohama, A., et al. 2016, *ApJ*, 820, 26
- Fukui, Y., Tsuge, K., Sano, H., et al. 2017, *PASJ*, 69, L5
- Gruendl, R. A., & Chu, Y.-H. 2009, *ApJS*, 184, 172
- Hartmann, L. & Burkert, A. 2007, *ApJ*, 654, 988
- Herrera, C. N., Rubio, M., Bolatto, A. D., et al. 2013, *A&A*, 554, A91
- Habe, A., & Ohta, K. 1992, *PASJ*, 44, 203
- Hartmann, L. & Burkert, A. 2007, *ApJ*, 654, 988
- Hill, T., André, P., Arzoumanian, D., et al. 2012, *A&A*, 548, L6
- Hollenbach, D., & Salpeter, E. E. 1971, *ApJ*, 163, 155
- Inoue, T., & Fukui, Y. 2013, *ApJL*, 774, L31
- Inoue, T., & Inutsuka, S.-i. 2012, *ApJ*, 759, 35
- Inoue, T., Hennebelle, P., Fukui, Y., et al. 2018, *PASJ*, 70, S53
- Inutsuka, S., & Miyama, S., 1997, *ApJ*, 480, 681

- Johansson, L. E. B., Greve, A., Booth, R. S., et al. 1998, *A&A*, 331, 857
- Jura, M. 1974, *ApJ*, 191, 375
- Kim, S., Dopita, M. A., Staveley-Smith, L., & Bessell, M. S. 1999, *AJ*, 118, 2797
- Kim, S., Staveley-Smith, L., Dopita, M. A., et al. 2003, *ApJS*, 148, 473
- Krumholz, M. R., Klein, R. I., McKee, C. F., Offner, S. S. R., & Cunningham, A. J. 2009, *Science*, 323, 754
- Larson, R. B. 1981, *MNRAS*, 194, 809
- Matsumoto, T., Dobashi, K., & Shimoikura, T. 2015, *ApJ*, 801, 77
- McMullin, J. P., Waters, B., Schiebel, D., Young, W., & Golap, K. 2007, in *ASP Conf. Ser. 376, Astronomical Data Analysis Software and Systems XVI*, ed. R. A. Shaw, F. Hill, & D. J. Bell (Tucson, AZ: Univ. Arizona Press), 127
- Minamidani, T., Mizuno, N., Mizuno, Y., et al. 2008, *ApJS*, 175, 485
- Minamidani, T., Tanaka, T., Mizuno, Y., et al. 2011, *AJ*, 141, 73
- Mizuno, A., Onishi, T., Yonekura, Y., et al. 1995, *ApJL*, 445, L161
- Motte, F., Bontemps, S., Schilke, P., et al. 2007, *A&A*, 476, 1243
- Myers, P. C. 2009, *ApJ*, 700, 1609
- Nagahama, T., Mizuno, A., Ogawa, H., & Fukui, Y. 1998, *AJ*, 116, 336
- Nayak, O., Meixner, M., Fukui, Y., et al. 2018, *ApJ*, 854, 154
- Nguyen-Lu'o'ng, Q., Motte, F., Carlhoff, P., et al. 2013, *ApJ*, 775, 88
- Palmeirim, P., André, P., Kirk, J., et al. 2013, *A&A*, 550, A38
- Peretto, N., Fuller, G. A., Duarte-Cabral, A., et al. 2013, *A&A*, 555, A112
- Saigo, K., Onishi, T., Nayak, O., et al. 2017, *ApJ*, 835, 108
- Schaefer, B. E. 2008, *AJ*, 135, 112
- Schneider, N., Csengeri, T., Bontemps, S., et al. 2010, *A&A*, 520, A49
- Seale, J. P., Meixner, M., Sewilo, M., et al. 2014, *AJ*, 148, 124
- Shima, K., Tasker, E. J., Federrath, C., & Habe, A. 2017, 70, S54
- Takahira, K., Tasker, E. J., & Habe, A. 2014, *ApJ*, 792, 63
- Tan, J. C., Beltrán, M. T., Caselli, P., et al. 2014, in *Protostars and Planets VI*, ed. H. Beuther et al. (Tucson, AZ: Univ Tucson Press), 149
- Testor, G., Lemaire, J. L., Field, D., et al. 2006, *A&A*, 453, 517
- Tokuda, K., Onishi, T., Saigo, K. et al. 2018, *ApJ*, 826, 8
- Torii, K., Hattori, Y., Hasegawa, K., et al. 2017, *ApJ*, 835, 142
- Williams, G. M., Peretto, N., Avison, A., Duarte-Cabral, A., & Fuller, G. A. 2018, *A&A*, 613, A11
- Zinnecker, H., & Yorke, H. W. 2007, *ARA&A*, 45, 481